Reduction of fatigue loads on jacket substructure through blade design optimization for multimegawatt wind turbines at 50 m water depths

NJOMO WANDJI, Wilfried; Pavese, Christian; Natarajan, Anand; Zahle, Frederik

Published in:
Journal of Physics: Conference Series (Online)

Link to article, DOI:
10.1088/1742-6596/753/4/042022

Publication date:
2016

Document Version
Publisher's PDF, also known as Version of record

Reduction of fatigue loads on jacket substructure through blade design optimization for multi-megawatt wind turbines at 50 m water depths

2016 J. Phys.: Conf. Ser. 753 042022

(http://iopscience.iop.org/1742-6596/753/4/042022)

Reduction of fatigue loads on jacket substructure through blade design optimization for multi-megawatt wind turbines at 50 m water depths

W Njomo Wandji[1,2], C Pavese[1], A Natarajan[1] and F Zahle[1]

[1] DTU Wind Energy, Technical University of Denmark, Frederiksborgvej 399, DK-4000 Roskilde, Denmark
[2] Author to whom any correspondence should be addressed. wilw@dtu.dk, tel.: +45 9351 1501

Abstract. This paper addresses the reduction of the fore-aft damage equivalent moment at the tower base for multi-megawatt offshore wind turbines mounted on jacket type substructures at 50 m water depths. The study investigates blade design optimization of a reference 10 MW wind turbine under standard wind conditions of onshore sites. The blade geometry and structure is optimized to yield a design that minimizes tower base fatigue loads without significant loss of power production compared to that of the reference setup. The resulting blade design is then mounted on a turbine supported by a jacket and placed under specific offshore site conditions. The new design achieves alleviate fatigue damage equivalent loads also in the jacket members, showing the possibility to prolong its design lifetime or to save material in comparison to the reference jacket. Finally, the results suggest additional benefit on the efficient design of other components such as the constituents of the nacelle.

1. Introduction

Recent trends in offshore wind energy have resulted in the need for the design of multi-megawatt wind turbines at moderate water depths (up to 50 m). In such environments, adequate fixed support structures, which are capable of withstanding the extreme and fatigue loads throughout the design lifetime, are required. Kallehave et al. [1] have inventoried monopile, bucket, and jacket concepts as typical fixed support structures. In particular, jackets attract much interest for their competitiveness at 50 m water depths, their ease of installation, and their relative independence to soil properties, which can facilitate their mass production for a given wind farm. Yet, the jacket solution can be extremely challenging to ensure durability for 25 years with respect to its fatigue limit state for multi-megawatt wind turbines [2].

Fatigue loads on a jacket result from the contributions of sea, wake turbulence, and rotor induced loadings. The latter two contributions can be alleviated by selecting appropriate load mitigating control algorithms and/or appropriate blade aerodynamic designs.

This paper addresses design optimization of the blades in order to maintain fatigue lifetime of a jacket at 50+ m water depths for a 10 MW wind turbine with least material cost. The specific goal is to minimize the fore-aft damage equivalent moments while limiting the amplitude of the side-side moments. The study case for the application of the developed optimization algorithm consists of a reference turbine [3] mounted on a reference jacket [2]. The optimization is carried out on standard

wind conditions of onshore sites, but its results are applied on specific offshore site conditions to show that the optimized blades can be used for general site conditions.

2. Site conditions, reference turbine and jacket

2.1. Metocean conditions and soil profile

The jacket mounted turbine is assumed to be located at a site whose specific metocean conditions are given in table 1 [2]. The operational wind range is divided into 11 mean wind speed bins, based on which load simulations are carried out under normal turbulence conditions. Each mean wind speed bin is linked to a particular sea state characterized by an expected significant wave height and a peak spectral period. The wave height is modelled based on Pierson-Moskowitz spectrum at the expected value of the sea state characteristics conditional on the mean wind speed.

The soil profile is also taken from Ref [2]. The soil consists of superimposed sand layers whose submerged weight varies between 9.00 kN/m^3 and 11.00 kN/m^3; and the characteristic angle of internal friction is equal to 35.0°. The complete description of the soil properties is not presented here in details because of its limited influence in the present study.

Table 1. Site specific metocean conditions.

Mean wind speed [m/s]	Normal turbulence intensity [%]	Significant wave height, Hs [m]	Peak period, Tp [s]	Expected annual frequency [hrs/yr.]
5	18.95	1.140	5.820	933.75
7	16.75	1.245	5.715	1087.30
9	15.60	1.395	5.705	1129.05
11	14.90	1.590	5.810	1106.75
13	14.40	1.805	5.975	1006.40
15	14.05	2.050	6.220	820.15
17	13.75	2.330	6.540	633.00
19	13.50	2.615	6.850	418.65
21	13.35	2.925	7.195	312.70
23	13.20	3.255	7.600	209.90
25	13.00	3.600	7.950	148.96

2.2. Structure: turbine and jacket

The DTU 10 MW reference wind turbine (DTU 10 MW RWT) [3] is considered mounted on the jacket substructure. The DTU 10 MW RWT is a variable speed pitch controlled conceptual offshore wind turbine, whose design parameters are summarized in table 2. The control system used for the DTU 10 MW RWT has been slightly changed and enriched with an exclusion zone option when operating on the jacketed turbine. The jacket (see figure 1) is a 4-legged spatial truss like structure founded on four piles and connected to the tower bottom through a transition piece. Its key parameters are given in Ref [2].

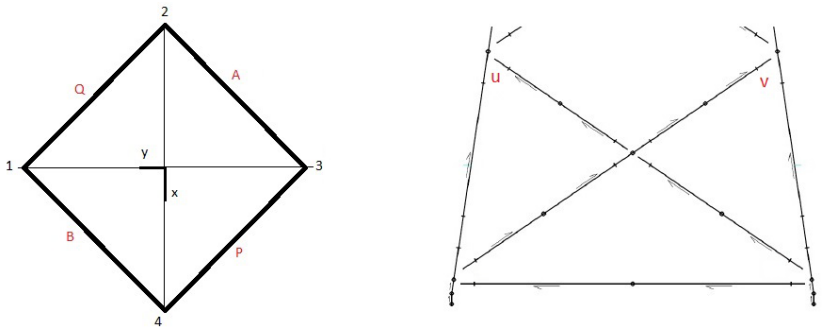

Figure 1. Geometry of the jacket. (Left) plan view with sides' names. (Right) nomenclature of the selected hotspots on a typical jacket's side. A joint's name is made of the side's name (A, B, P, or Q) and the joint's position (u or v). For example, joint's names can be Au, Pv etc.

Table 2. Key design parameters of the DTU 10 MW RWT [3].

Parameters	Values
Wind regime	(see table 1)
Rotor type, orientation	3 bladed - Clockwise rotation – Upwind
Control	Variable speed – Collective pitch
Cut-in, rated, cut-out wind speed	4 m/s, 11.4 m/s, 25 m/s
Rated power	10 MW
Rotor, hub diameter	178.3 m, 5.6 m
Hub height	119.0 m
Drivetrain	Medium speed, Multiple-stage Gearbox
Minimum, maximum rotor speed	6.0 rpm, 9.6 rpm
Maximum generator speed	480.0 rpm
Gearbox ratio	50
Maximum tip speed	90.0 m/s
Hub overhang	7.1 m
Shaft tilt, coning angle	5.0°, -2.5°
Blade prebend	3.3 m
Rotor mass including hub	227,962 kg
Nacelle mass	446,036 kg
Tower mass	628,442 kg

3. Fully coupled aero-hydro-servo-elastic analysis

3.1. Fully integrated simulation

To ensure that all ambient interactions are adequately considered, a fully coupled design load computation was carried out using the aero-hydro-servo-elastic software package HAWC2 [4]. HAWC2 utilizes a multibody formulation, which couples different elastic bodies together using Timoshenko beam finite elements [5] whereby their stiffness, mass, and damping are assembled into the governing equations of motion coupled to aerodynamic forces, whose time domain solution is obtained using the Newmark-β method [6]. The damping coefficients are specified using Rayleigh coefficients to obtain desired damping ratios for the global structure. The blade element momentum theory supplemented with Leishman-Beddoes dynamic stall model and dynamic inflow is employed to represent the rotor unsteady aerodynamics [7]. The turbulent wind field in the aeroelastic simulations is defined using the Mann model [8]. Random Gaussian 10-minute turbulent wind realizations are used as input to simulate normal operation over the 11 mean wind speed bins and storm conditions.

The irregular wave height is modelled using a Pierson-Moskovitz spectrum at the expected value of significant wave height and spectral peak period at each mean wind speed. In fact, the Pierson-Moskowitz type is used for fatigue load case because of its spread spectral, which allows a better energy distribution. Random wave kinematics are computed according to the linear Airy model with Wheeler stretching [9].

The interaction between the soil and the piles are modelled based on p-y curves and t-z curves, which consider piles as Winkler beams according to API RP2A WSD [10]. The pile toes are restrained against vertical displacement (no Q-z curve was considered) and against yaw movement.

3.2. Design load case

A design load case, DLC 1.2 as defined by IEC 61400-3 [11] is considered herein for fatigue limit state. DLC 1.2 is the load case under normal operation to account for fatigue damage over the turbine lifetime. A total of 11 wind speed bins (from 5 m/s to 25 m/s with 2 m/s step) with one wind turbulence seed each are considered. Further 16 combinations of the rotor direction around the jacket are considered with the wind aligned to or with yaw errors of ±8° from the normal to the rotor plane.

The waves are aligned to the wind direction. This set of conditions provides 11 × 1 × 3 × 16 = 528 scenarios.

4. Fatigue limit state

4.1. Damage equivalent loads

The damage equivalent load can be defined as the load that can cause the same amount of fatigue if it were applied an equivalent number of cycles. Given a time series of a load, L, it can be calculated as:

$$L_{eq} = \int_{V_{in}}^{V_{out}} p(V) \int_{\Delta L_a}^{\Delta L_b} \left(\frac{n(\Delta L|V)\Delta L^m}{N_{eq}} \right)^{1/m} \mathrm{d}\Delta L \, \mathrm{d}V \quad (1)$$

where

$p(V)$ is the probability of occurrence of the wind speed V;
$n(\Delta L|V)$ is the number of the load ranges ΔL given V, obtained after rainflow counting;
N_{eq} is the equivalent number of cycles during the structure lifetime, $N_{eq} = 10^7$; and
m is the Wohler parameter, $m = 4$.

The change in damage equivalent load from the reference setup to a new one is obtained by $\Delta(L_{eq}) = L_{eq}^{new}(L_{eq}^{ref})^{-1} - 1$.

4.2. Fatigue lifetime

The fatigue lifetime is evaluated at several hotspots located at the K-joints between the legs and the lower braces. The hotspots are selected based on the previous studies [2], which have identified them as the weakest structural points. For a given welded connections, stress time series are calculated at eight points around the circumferences of each side; they are obtained by multiplying the nominal stresses by the stress concentration factors (SCFs) estimated by the Efthymiou's equations [12]. The design stress time series are calculated as:

$$\sigma_d = \gamma_x \, \gamma_f \, \gamma_m \, \gamma_n \, SCF \, \sigma_{nominal} \quad (2)$$

where the partial safety factors are taken from Sorensen and Toft (2014) [13]: γ_m = 1.25, γ_c = 1.10, and γ_f = 1.20 are associated to the material properties, to the component's consequence of failure, and to the fatigue stress range counting, respectively. γ_x is an additional partial safety factor associated with the uncertainties in the stress concentration factors, corrosion, marine growth etc. The stress ranges are obtained from the rainflow counting method applied on the design stress time series. The number of cycles, $N(\Delta\sigma)$, corresponding to full damage induced by a given stress range, $\Delta\sigma$, is obtained by the design S-N curve for tubular member in seawater with cathodic protection as per DNV RP C203 [12], which is described as:

$$\log N = \log \bar{a} - m \log \left[\Delta\sigma \left(\frac{t}{t_{ref}} \right)^k \right] \quad (3)$$

where

m and $\log \bar{a}$ = are respectively the negative inverse slope of the S-N curve and the intercept of log N axis. For S-N curves of T-type in seawater with cathodic protection, (m = 3, $\log \bar{a}$ = 11.764) for $N \leq 10^6$, and (m = 5, $\log \bar{a}$ = 15.606) for $N > 10^6$;
t_{ref} = is the reference thickness equal to 32 mm;
t = is the thickness through which the crack will most likely grow; $t = t_{ref}$ if $t < t_{ref}$;
k = is the thickness exponent on fatigue strength. k = 0.25 for $SCF < 10.0$ and k = 0.30 for $SCF > 10.0$.

Then, Palmgren Miner's rule [14] is applied to accumulate the induced damage. During one year, the accumulated damage is expressed as [15]:

$$D_1 = \gamma_{DF} \frac{T_1}{T} \int_{V_{in}}^{V_{out}} \int_{\Delta\sigma_A}^{\Delta\sigma_B} \frac{n(\Delta\sigma|V,T)}{N(\Delta\sigma)} \, p(V) \, \mathrm{d}\Delta\sigma \, \mathrm{d}V \tag{4}$$

where $\gamma_{DF} = 3.0$ is the fatigue reserve factor associated with lack of possibility for inspections, T_1 is the number of seconds in one year, $T = 600\ s$ is the simulation duration, $N(\Delta\sigma)$ is the number of cycles that can cause full damage under the stress range $\Delta\sigma$, $n(\Delta\sigma|V,T)$ is the actual yearly number of cycles corresponding to the stress range $\Delta\sigma$, given a wind speed V and the simulation duration T, and $p(V)$ is the probability of occurrence of the wind speed V. Based on the one year accumulated fatigue damage, the fatigue lifetime in years is obtained by $L_f = D_1^{-1}$. Finally, the change in fatigue lifetime from the reference setup to a new one is computed as $\Delta(L_f) = L_f^{new}(L_f^{ref})^{-1} - 1$.

5. Rotor blade optimization process

The blade optimization process is carried by the HAWTOpt2 framework [16]. Built on the OpenMDAO (Open-source Multidisciplinary Design, Analysis, and Optimization Framework) [17][18][19][20], the tool is used to handle the definition of the optimization problem, workflow, dataflow and parallelization of simulation cases. OpenMDAO provides an interface to PyOpt [21], a container for several optimization algorithms. In this work, the gradient-based sequential quadratic programming optimizer SNOPT is used. A full description of the framework and its application on aeroelastic optimization of a wind turbine is provided in ref. [16].

5.1. Problem definition and methodology

The description of the numerical optimization problem and characterization of the HAWTOpt2 workflow, its components, and the tools used are detailed in ref. [16]. The fundamental difference herein from the design problem depicted in [16] is the definition of the objective function. In the current work, the objective function is a compound objective consisting of tower base fore-aft damage equivalent load (DEL) and the blade first mass moment:

$$f\left(\{\boldsymbol{x_p}, \boldsymbol{x_s}\}, \mathbf{p}, w\right) = (1-w)\frac{M_m(\{\boldsymbol{x_p},\boldsymbol{x_s}\},\mathbf{p})}{M_m(\{\mathbf{0},\mathbf{0}\},\mathbf{p})} + w\frac{DEL(\{\boldsymbol{x_p},\boldsymbol{x_s}\},\mathbf{p})}{DEL(\{\mathbf{0},\mathbf{0}\},\mathbf{p})} \tag{5}$$

where

f = is the objective function depending on a set of planform variables $\boldsymbol{x_p}$, a set of structural variables $\boldsymbol{x_s}$, both described in table 3, a set of constant parameters $\mathbf{p}$, which includes all the characteristics of the DTU 10 MW RWT reported in [3], and a weight w, that defines toward which of the elementary objectives the optimization is biased;

$M_m(\{\mathbf{0},\mathbf{0}\},\mathbf{p})$= is the reference blade mass moment;

$DEL(\{\mathbf{0},\mathbf{0}\},\mathbf{p})$= is the reference tower base fore-aft damage equivalent load.

The constraints of the optimization problem cover various criteria:

(a) **Planform**: the maximum tip sweep is limited to be lower than maximum chord for transport;
(b) **Geometry**: material thickness is lower-bound to ensure that the layups have realistic thicknesses depending on section region and material, and the ratio thickness-width is set above 0.08 to avoid spar cap buckling;
(c) **Strength**: The ultimate strain utilization ratio is set below one (inclusive of partial safety factors) to prevent material failure;
(d) **Aeroelasticity**: The annual energy production (AEP), the rotor thrust, the maxima tip deflections, the blade root DEL, and the tower base side-side are set to be at least as better than those of DTU 10 MW RWT. The operational lift coefficient is constrained to be below 1.35 along the

blade length to avoid stall. The aeroelastic frequency is set above 0.15 Hz to avoid resonance in three operational points.

As done in [21], free form deformation splines with numbers of control points (CPs) appropriate to the variable selected are used to parametrize the distribution of the design variables along the blade length.

Table 3. Design variables of the blade optimization problem.

Design Variables (DVs)	**CPs Spanwise Distribution**	**# of DVs**	**Comment**
Planform x_p			
Blade Sweep	[0.5, 0.85, 1.0]	3	Inner blade geometry fixed
Structure x_s			
Trailing edge uniax	[0.0, 0.1, 0.2]	3	Outer blade TE layups fixed. Pressure/suction side
Trailing edge triax	[0.0, 0.1, 0.2]	3	Outer blade TE layups fixed. Pressure/suction side
Trailing panel triax	[0.0, 0.1, 0.2, 0.5, 0.85, 1.0]	6	Pressure/suction side
Spar cap uniax	[0.0, 0.1, 0.2, 0.5, 0.85, 1.0]	6	Pressure/suction side
Leading panel triax	[0.0, 0.1, 0.2, 0.5, 0.85, 1.0]	6	Pressure/suction side
Leading edge uniax	[0.0, 0.1, 0.2, 0.5, 0.85, 1.0]	6	Pressure/suction side
Leading edge triax	[0.0, 0.1, 0.2, 0.5, 0.85, 1.0]	6	Pressure/suction side
Upper cap position	[(0, 0.2), 0.40, 0.75]	6	Inner CPs grouped, tip position fixed. Two points defined.
Lower cap position	[(0, 0.2), 0.40, 0.75]	6	Inner CPs grouped, tip position fixed. Two points defined.
Total		**51**	

5.2. Resulting blade characteristics and comparison of the two blade sets

The optimal blade is selected from a series of designs with varying bias towards either tower base fore-aft DEL or blade mass moment. Figure 2 shows the Pareto front used to select the optimal design. The chosen design is the FMxeq_N0.75, as it achieves the best tower base fore-aft load alleviation.

A comparison of the baseline and the optimized blade layups is provided in figure 3. The thickness of the uniaxial plies of the caps is increased compared to the baseline, especially in the central part of the blade. Although these changes lead to an increase of about 4% of the blade total mass, the reduced blade mass moment helps reducing the tower base side-side moment, as reported in the next section.

The tower base fore-aft DEL alleviations are achieved through bend-twist coupling effects implemented in the optimal design varying the blade geometry (sweep) and the location of the caps. The plots on the left side of figure 4 show a comparison between the location of the caps of the baseline blade and the location of the caps of the optimized blade. On the right side of the figure, the changed geometry of the optimized blade is highlighted. The blue lines depict the structural pitch of the baseline and the optimized blade, while the red ones show the x-coordinate of the centerline.

The twist of the planform has not been included in the DVs. For this reason, to compensate for the loss of AEP below rated wind speed, the optimizer sweeps the tip of the blade forward, so to induce a bend-twist coupling toward stall. The angle of attack at the tip of the blade increases, enhancing the AEP when the energy needs to be harvest toward the outer part of the rotor (below rated wind speed). The middle part of the blade is swept backward to create a bend-twist coupling toward feather, reducing the loads above rated wind speed, when the inner part of the rotor has to sustain the greatest loading. The disposition of the caps helps enhancing these effects.

To ensure stability of the optimized blade planform, an open-loop eigenvalue analysis is performed to check aero-elastic frequencies and damping of the first 10 wind turbine modes of the onshore model. Using the linearized model implemented in HAWCStab2 [22], figure 5 shows the aero-elastic

frequencies (left plot) and damping ratios (right plot) for the baseline DTU 10 MW RWT and the wind turbine with optimized blades.

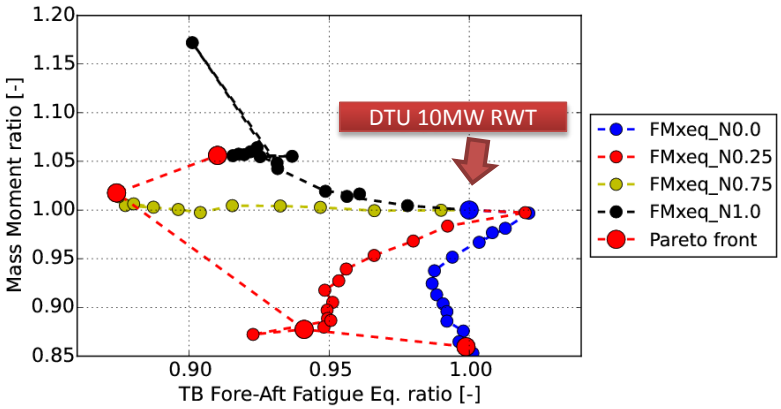

Figure 2. Pareto front for optimization of the DTU 10 MW RWT blade. The objective function aims at minimizing tower base fore-aft LTEFL and at minimizing blade mass moment. The compound objective is biased according to 4 weights: 0.0, 0.25, 0.75, 1.0, where 0.0 is full minimization of the blade mass moment.

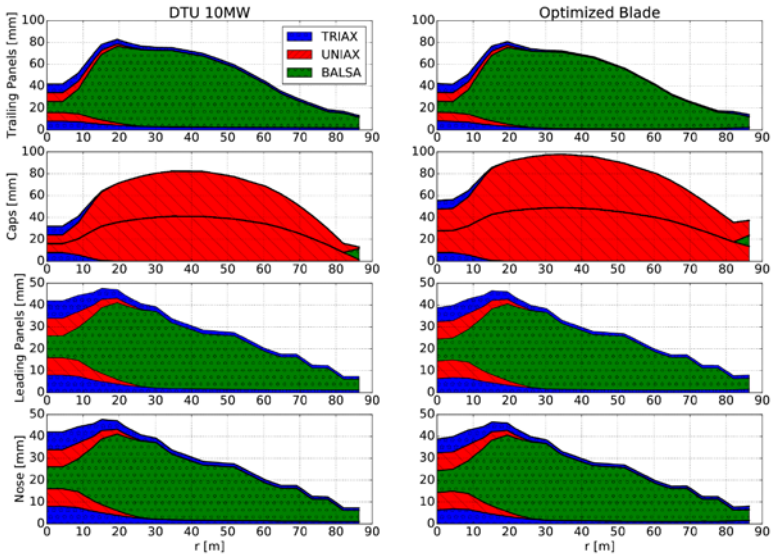

Figure 3. Comparison between the baseline blade layups (left) and optimized blade layups (right).

Baseline

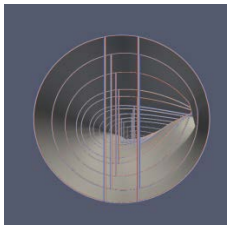

Optimized Blade

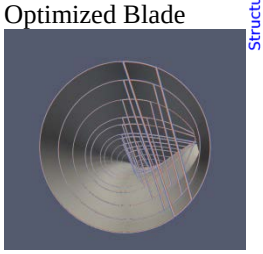

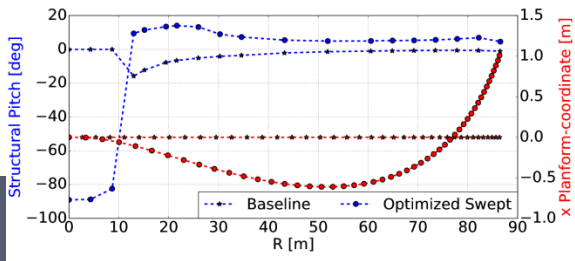

Figure 4. Comparison between baseline and optimized blade. (Left) close up to highlight the location of the caps. (Right) comparison between the blade geometries. Blue dashed lines represent the structural pitch axis, while the red ones is the x-coordinate of the centreline.

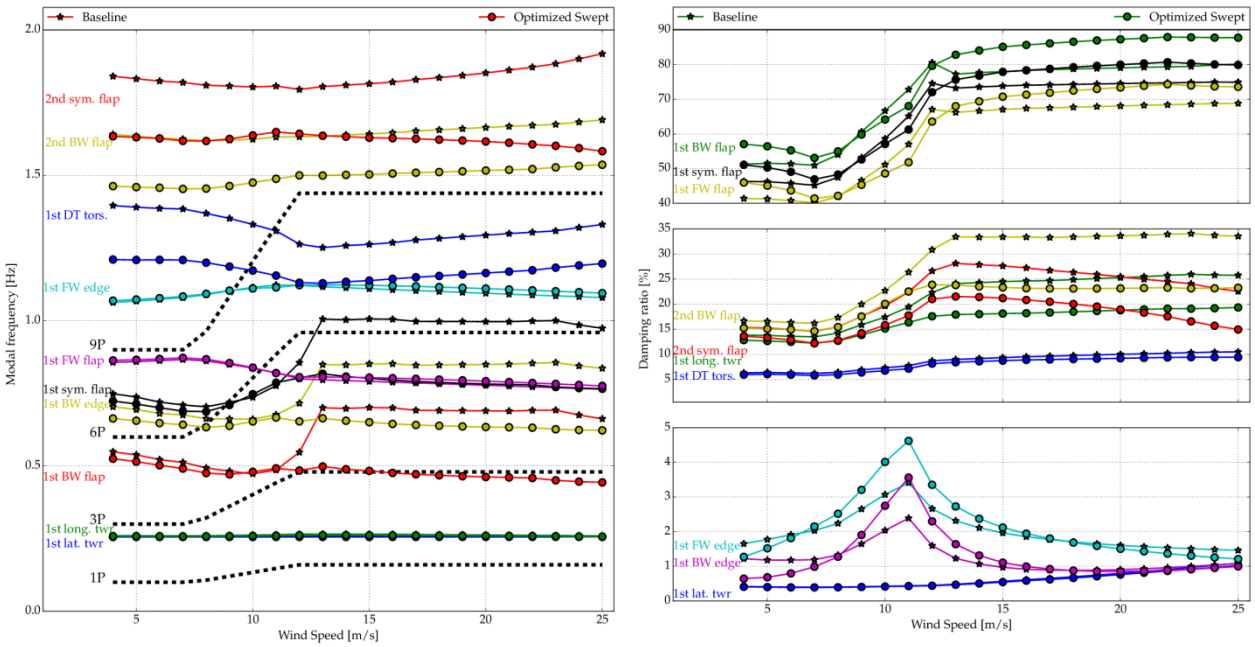

Figure 5. Open-loop aero-elastic frequencies (left plot) and damping ratios (right plot) of the first 10 wind turbine modes of the baseline design and the optimized one. In the left plot, 1P, 3P, 6P, and 9P frequencies are highlighted with black dash lines.

The edgewise whirling aero-elastic frequencies are kept away from resonance (especially 6P), due to the constraints introduced in the MDO and described in table 3. No negatively damped modes are registered, even though the first edgewise whirling modes of the optimized turbine are lower than the baseline at low wind speeds, presenting very low damping ratios.

6. Results and discussions

The DTU 10 MW RWT is mounted on the reference jacket at 50 m water depth with the same hub height i.e. 119 m above the mean sea level. Three setups are considered:

- The DTU 10 MW RWT, with the reference blades and the reference control system, placed on land;
- The DTU 10 MW RWT, with the reference blades and the augmented control system, placed at 50 m water depth; and
- The DTU 10 MW RWT, with the optimized blades and the augmented control system, placed at 50 m water depth.

6.1. Performance check

The respective key properties at the system level of the two jacketed setups are compared versus those of the DTU 10 MW RWT using three criteria: natural frequencies, energy production, and thrust force. Table 4 presents the respective natural frequencies for the three setups. It can be seen that the jacket substructure significantly modifies the first modes of the setups, which are the first bending modes of the support structure.

Besides, figure 6 illustrates some characteristic curves for the three setups. On the left side, the respective power curves are shown. Globally, the power curves show that the levels of production are similar with either structure, notwithstanding the insignificant reduction of the energy production observed around the rated wind speed with the optimized blade set. On the right side of figure 5, the respective aerodynamic rotor curves are plotted. The optimized blade setup achieves to reduce the rotor thrust force from about 1600 kN with the reference blades to about 1450 kN, i.e. about 9.4 %

less. This reduction is beneficial to the entire structure, which includes the nacelle's components and the support structure.

Table 4. Respective natural frequencies [Hz] of the three setups.

Mode	Onshore model	Offshore model with reference blades	Offshore model with optimized blades
Mode 1	0.25125	0.28779	0.28728
Mode 2	0.25620	0.29503	0.29407
Mode 3	0.54671	0.54974	0.55106
Mode 4	0.58937	0.59212	0.58767
Mode 5	0.62971	0.63236	0.61764

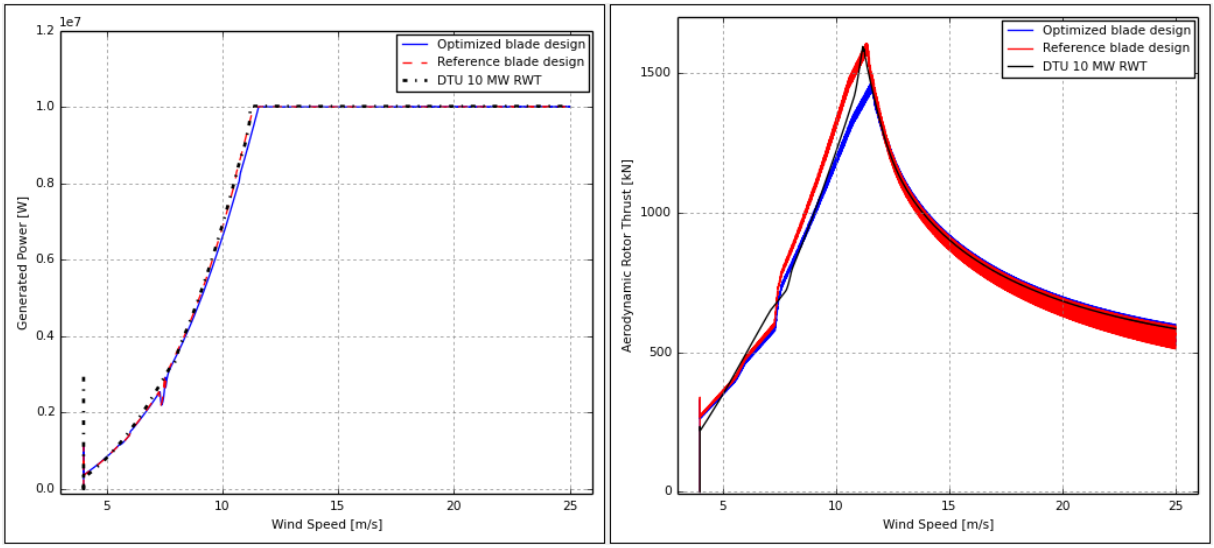

Figure 6. Characteristic curves for each setup. (Left) power curve. (Right) aerodynamic rotor thrust.

6.2. Damage equivalent loads at the tower bottom

The damage equivalent loads (forces and moments) are computed according to equation 1 at the interface between the tower bottom and the transition piece. The results are displayed on figure 7, which shows a decrease of all loads for the optimized blade setup.

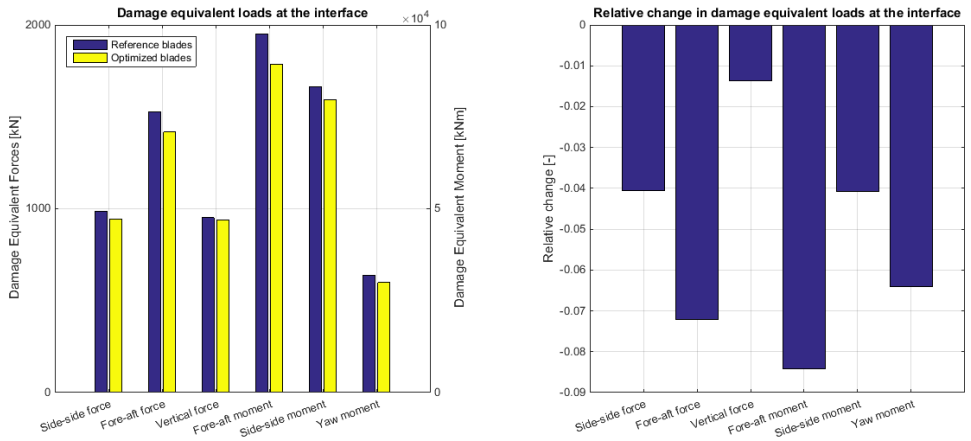

Figure 7. Effect of the blade optimization on the damage equivalent load at the interface. Due to blade optimization, all loads are reduced (right) with a relative change varying from 1.4 % to 8.4 % (left).

Particularly, the fore-aft damage equivalent moment has been reduced from 97,482 kNm to 89,269 kNm, which corresponds to 8.4 % reduction. In general, the reductions range from 1.4 % to 8.4 %, which translate in fatigue lifetime extension of the jacket substructure as shown in the next section. The similarity of the turbine natural frequencies between the new rotor and the baseline indicates that the damage equivalent load reductions are primarily due to the optimized blades.

6.3. Jacket lifetime extension

Fatigue lifetime change is computed with the results of the load simulations at the selected hotspots (see figure 1) on the jacket for the cases with the reference blades and with the optimized blades. Figure 8 shows that the hotspots' expected fatigue lifetimes have been extended by a relative change varying between 33.3 % and 125 %, approximately. This means that, due to the optimized blade set, the minimum lifetime of the overall jacket can be improved at the critical hotspots, and steel material can be saved at other hotspots that were already satisfying the fatigue limit state. Thus, it results a combination of material saving and lifetime extension.

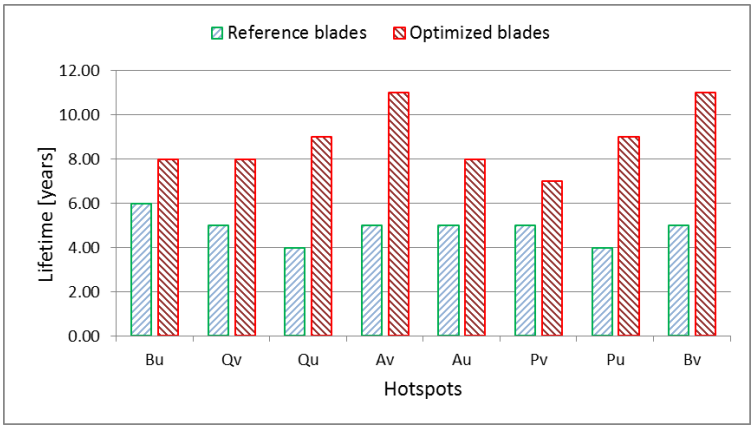

Figure 8. Improvement in fatigue lifetime at selected hotspots.

7. Conclusion

In conclusion, an aeroelastically tailored blade design is proposed with the goal of reducing the fore-aft fatigue moment at the tower base; the ultimate aim being to prolong the fatigue lifetime of the jacket substructure and/or reduce material cost. Based on a reference turbine, the optimization was carried out based on standard onshore site conditions, and the resulting blade design was mounted on a jacket supported turbine placed at specific offshore site conditions. The study has revealed three main inferences:

i. It is computationally efficient to carry out the optimization process on a (simple) land turbine subjected to standard wind conditions, and then to adapt the resulting design on a (complex) offshore turbine subjected to site specific metocean conditions.
ii. Altogether with the fore-aft fatigue moment, all other fatigue loads at the tower base as well as loads at the tower top have been alleviated without a significant loss of power production. The load reduction is beneficial to the efficient design of all wind turbine's modules, which include nacelle's components and support structure.
iii. The reduction of fatigue loads at the tower bottom has been translated, for the jacket substructure (which for an offshore turbine has the largest CAPEX contribution), in fatigue lifetime extension at every selected hotspot, which allows material cost saving.

In the light of these encouraging results, further attention can be given to possibility to couple this innovative design process to other load mitigation techniques, whether active or passive.

Acknowledgments
The research leading to these results has received funding from the European Community's 7th Framework Programme FP7-ENERGY-2012-1-2STAGE project INNWIND.EU under grant agreement No. 308974. The financial support is greatly appreciated.

References
[1] Kallehave D, Byrne B W, LeBlanc Thilsted C and Mikkelsen K K 2015 Optimization of monopiles for offshore wind turbines. *Phil. Trans. R. Soc*. A **373**. 1-15
[2] Von Borstel T 2013 INNWIND Design Report Reference Jacket. Ramboll. http://www.innwind.eu/-/media/Sites/innwind/Publications/Deliverables/DeliverableD4,-d-,31_20131030_INNWIND,-d-,EU.ashx?la=da
[3] Bak C, Zahle F, Bitsche R, Kim T, Yde A, Henriksen L C, Andersen P B, Natarajan A and Hansen M H 2013 Design and performance of a 10 MW wind turbine. http://www.innwind.eu/-/media/Sites/innwind/Publications/Deliverables/DeliverableD1,-d-,21ReferenceWindTurbinereport_INNWIND,-d-,EU.ashx?la=da
[4] Larsen T J and Hansen A M 2014 *How 2 HAWC2, the user's manual*. (Risoe: DTU Wind Energy)
[5] Przemieniecki J S 1968 *Theory of matrix structural analysis* (New York: McGraw-Hill Book Company)
[6] Chopra A K 2011 *Dynamics of Structures: Theory and Applications to Earthquake Engineering* 4th ed. (Pearson)
[7] Manwell J F, McGowan J G and Rogers A L 2009 *Wind Energy Explained: Theory, Design and Application* 2nd ed (John Wiley and Sons, Ltd)
[8] Mann J 1994 *The spatial structure of neutral atmospheric surface-layer turbulence* Journal of Fluid Mechanics 273:141–68
[9] Chakrabarti S 2005 *Handbook of Offshore Engineering* (Amsterdam: Elsevier)
[10] American Petroleum Institute 2005 *Recommended practice for planning, designing and constructing fixed offshore platforms—Working stress design* API RP2A WSD
[11] The international Electrotechnical Commission 2009 *Wind Turbines – Part 3: Design requirements for offshore wind turbines* IEC 61400-3 Ed 1
[12] Det Norske Veritas 2011 *Fatigue Design of Offshore Steel Structures – Recommended Practice* DNV-RP-C203
[13] Sorensen J D, Toft H S 2014 *Safety Factors – IEC 61400-1 ed. 4 – Background document*. (Risoe: DTU Wind Energy)
[14] Miner A M 1945 *Cumulative damage in fatigue* Journal of Applied Mechanics **12**, A159-A164
[15] The international Electrotechnical Commission 2009 *Wind Turbines – Part 1: Design requirements* IEC 61400-1 Ed 3
[16] Zahle F, Tibaldi C, Verelst D R, Bak C, Bitche R and Blasques J P A A 2015 *Aero-Elastic Optimization of a 10 MW Wind Turbine* (Kissimmee, Florida: AIAA SciTech - 33rd Wind Energy Symposium)
[17] http://openmdao.org, 2012
[18] Moore K T, Naylor B A and Gray J S 2008 *The Development of an Open-Source Framework for Multidisciplinary Analysis and Optimization* (Victoria, Canada: 10th AIAA/ISSMO Multidisciplinary Analysis and Optimization Conference)
[19] Gray J S, Moore K T and Naylor B A 2010 *OpenMDAO An Open Source Framework for Multidisciplinary Analysis and Optimization*, http://www.aric.or.kr/treatise/journal/content.asp?idx=134451, (Fort Worth, Texas: 13th AIAA/ISSMO Multidisciplinary Analysis and Optimization Conference)
[20] Heath C M and Gray J S 2012 *OpenMDAO: Framework for Flexible Multidisciplinary Design, Analysis and Optimization Methods* (Honolulu, Hawaii: 8th AIAA Multidisciplinary Design Optimization Specialist Conference) pp 1–13
[21] http://pyopt.org/
[22] Hansen M H 2011 *Aeroelastic properties of backward swept blades* (Orlando, Florida: Proceedings of the 49th AIAA Aerospace Sciences Meeting)